Measurement of Velocity Profiles in Multiphase Flow using a Multi-Electrode Electromagnetic Flow Meter

T. Leeungculsatien[a] and G.P. Lucas[a]

[a] School of Computing and Engineering, University of Huddersfield, Huddersfield HD1 3DH, UK

E-mail: g.lucas@hud.ac.uk

ABSTRACT

A Helmholtz coil is used to produce a near-uniform magnetic field orthogonal to both the flow direction and the plane of an electrode array mounted on the internal surface of a non-conducting pipe wall. Induced voltages acquired from the electrode array are related to the flow velocity distribution via variables known as 'weight values' which are calculated using finite element software. Matrix inversion is used to calculate the velocity distribution in the flow cross section from the induced voltages measured at the electrode array. Experimental results are also presented for the reconstructed velocity profile of the continuous water phase in an inclined solids-in-water multiphase flow for which the axial water velocity distribution is highly non-uniform. The results presented in this paper are most relevant to flows in which variations in the axial flow velocity occur principally in a single direction.

Keywords: Velocity profile, multi-electrode electromagnetic flow meter, multiphase flow.

1 INTRODUCTION

Large variations in the axial flow velocity can also occur in multiphase flows e.g. horizontal and upward inclined multiphase flows in which axial velocity variations occur principally in the direction of gravity, with the minimum axial velocity at the lower side of the inclined pipe and the maximum velocity at the upper side of the inclined pipe. A specific example of a multiphase flow which is of great interest to the oil industry is upward inclined oil-in-water flow [1]. Such flows are 'water continuous' and so the multiphase mixture is electrically conducting allowing the use of electromagnetic flow meters. However since the water velocity varies from a minimum at the lower side of the inclined pipe to a maximum at the upper side of the inclined pipe this causes erroneous readings from a conventional electromagnetic flow meter. Another flow of interest to the oil industry occurs during the drilling of inclined oil wells when rock cuttings flow co-currently with water based drilling mud. Mixture density variations in the flow cross section, caused by settling of the rock cuttings, can cause variations in the axial mud velocity from positive (upward) values at the upper side of the inclined well to negative (downward) values at the lower side. In view of the above, the objective of this paper is to describe a new non-intrusive electromagnetic flow metering technique for measuring the axial velocity profile of the conducting continuous phase of multiphase mixtures (such as horizontal and inclined oil-in-water flows and solids-in-water flows) in which the conductivity of the dispersed phase is very much lower than the conductivity of the continuous phase. [Note that in a previous paper [2] it has been shown that the relatively minor variations of fluid conductivity, which occur in the cross section of such multiphase flows, have only a minimal effect on the operation of electromagnetic flow meters. This is particularly true if the volume fraction of the non-conducting dispersed phase is less than about 0.4].

An alternative approach to accurate volumetric flow rate measurement in highly non-uniform single phase flows has been proposed by authors such Horner [3] and Xu et al [4] who described multi-electrode electromagnetic flow meters which are relatively insensitive to the flow velocity profile. However, this type of flow meter does not provide information on the local axial velocity distribution in the flow cross section. This can be a major drawback, particularly in a steady multiphase flow where, for example, the volumetric flow rate Q_c of a given phase can only be found by integrating the product of the steady local velocity v_c and the steady local volume fraction α_c of the phase in the flow cross section as follows

$$Q_c = \int_A v_c \alpha_c \, dA \tag{1}$$

where in equation 1 A refers to cross sectional area. The approach of Horner [3] would be of no benefit in determining the water volumetric flow rate in a highly inclined oil-in-water flow such as that described above – but in such a flow, the distribution of the local water velocity v_w could be determined using the electromagnetic flow metering method outlined in this paper and the distribution of the local water volume fraction α_w could be obtained non-intrusively using electrical resistance tomography (ERT) [5] enabling the water volumetric flow rate Q_w to be determined according to equation 1. Although previous work on velocity profile measurement using multi-electrode electromagnetic flow meters is reported in the literature (see for example [6] for a brief review) much of this previous work is not specifically aimed at multiphase flow measurement which is a major thrust of the work described in this paper. Also much of this previous work involves only simulations rather than the use of a practical device such as that described later in this paper.

The essential theory of electromagnetic flow meters (EMFMs) states that charged particles, in a conducting material which moves in a magnetic field, experience a Lorentz force acting in a direction perpendicular to both the material's motion and the applied magnetic field. Williams [7] applied a uniform transverse magnetic field perpendicular to the line joining the electrodes and the fluid motion and his experiments revealed that for a uniform velocity profile the flow rate is directly proportional to the voltage measured between the two electrodes. Subsequently Shercliff [8] showed that the local current density $\mathbf{j}$ in the fluid is governed by Ohm's law in the form of

$$\mathbf{j} = \sigma(\mathbf{E} + \mathbf{v} \times \mathbf{B}) \tag{2}$$

where σ is the local fluid conductivity, $\mathbf{v}$ is the local fluid velocity, and $\mathbf{B}$ is the local magnetic flux density. The expression $(\mathbf{v} \times \mathbf{B})$ represents the local electric field induced by the fluid motion, whereas $\mathbf{E}$ is the electric field due to charges distributed in and around the fluid. For fluids where the conductivity variations are relatively minor (such as the single phase and the multiphase flows under consideration in this paper) Shercliff [8] simplified equation 2 to show that the local potential U in the flow can be obtained by solving

$$\nabla^2 U = \nabla \cdot (\mathbf{v} \times \mathbf{B}) \tag{3}$$

For a circular cross section flow channel bounded by a number of electrodes, with a uniform magnetic field of flux density $\overline{B}$ normal to the axial flow direction, it can shown with reference to [8] that, in a steady flow, the potential difference U_j between the jth pair of electrodes is given by an expression of the form

$$U_j = \frac{2\overline{B}}{\pi a} \iint v(x,y) W(x,y)_j \, dx dy \tag{4}$$

where $v(x,y)$ is the steady local axial flow velocity at the point (x,y) in the flow cross section, $W(x,y)_j$ is the so-called 'weight value' relating the contribution of $v(x,y)$ to U_j and a is the internal radius of the flow channel. Equation 4 can be discretised as follows by assuming that the flow cross section can be divided into $\hat{I}$ elemental regions

$$U_j = \frac{2\overline{B}}{\pi a} \sum_{n=1}^{\hat{I}} \hat{v}_n \hat{W}_{n,j} \hat{A}_n \tag{5}$$

where $\hat{v}_n$ and $\hat{A}_n$ are respectively the local axial velocity in, and the cross sectional area of, the nth elemental region. $\hat{W}_{n,j}$ is the weight value describing the contribution of the axial velocity in the nth

elemental region to the jth potential difference U_j. If the axial flow velocity is now assumed to be constant in each of N large regions, equation 5 can be written as

$$U_j = \frac{2\overline{B}}{\pi a} \sum_{i=1}^{N} v_i \sum_{n=\hat{I}_{i-1}+1}^{\hat{I}_i} \hat{W}_{n,j} \hat{A}_n \tag{6}$$

where v_i is the axial flow velocity in the ith large region. In equation 6 when the subscript n is in the range $\hat{I}_{i-1}+1 \le n \le \hat{I}_i$ it refers to the elemental regions lying within the ith large region. [Note also that there are $\hat{I}_i - \hat{I}_{i-1}$ elemental regions within the ith large region and that, by definition, $\hat{I}_0 = 0$]. An 'area weighted' mean weight value w_{ij} relating the contribution of the velocity v_i in the ith large region to the jth potential difference U_j is given by

$$w_{ij} = \frac{\displaystyle\sum_{n=\hat{I}_{i-1}+1}^{\hat{I}_i} \hat{W}_{n,j} \hat{A}_n}{A_i} \tag{7}$$

where A_i is the cross sectional area of the ith large region. Combining equations 6 and 7 gives

$$U_j = \frac{2\overline{B}}{\pi a} \sum_{i=1}^{N} v_i w_{ij} A_i \tag{8}$$

It will be shown later in this paper that equation 8 can be inverted to enable estimates of the local axial flow velocity v_i in each of N large pixels to be determined from N potential difference measurements U_j made on the boundary of the flow. Furthermore, although equation 8 was derived on the assumption that the axial velocity in each large pixel is constant, it will be seen that when this inversion method is used to solve for the velocity in each large pixel then the values of v_i obtained give a good approximation to the mean axial velocity in each of the large pixels, in situations where there is some axial velocity variation within each large pixel.

In section 2 a practical EMFM is presented and in section 3 results obtained from this practical EMFM device in a multiphase flow are presented.

2 A PRACTICAL ELECTROMAGNETIC FLOWMETETING DEVICE

A real imaging electromagnetic flow meter (see Figure 1) was constructed. The non-conducting flow meter body, with an internal radius of 80mm, was made from Delrin. Four grooves on the flow meter body were machined to accommodate two circular coils which formed a Helmholtz coil, with the mean spacing between the two coils being equal to the mean coil radius. The electrode array contained 16 electrodes for measuring flow induced potential differences, with each electrode being made from stainless steel. Stainless steel was chosen because (i) it has high corrosion resistance and (ii) it has a low relative permeability which meant that the electrodes did not significantly affect the magnetic field in the flow cross section. Supports (labelled 'E' in Figure 1) were used to position the cables running between the electrodes and the detection circuitry in such a way that they were always parallel to the local magnetic field. This meant that any 'cable loops' were not cut by the time varying magnetic field - thus preventing non-flow-related potentials from being induced in the cables.
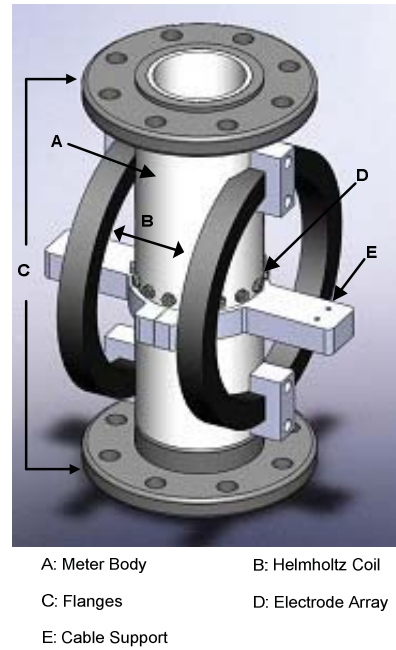
A: Meter Body   B: Helmholtz Coil

C: Flanges   D: Electrode Array

E: Cable Support

Figure 1: Design of the electromagnetic flow meter used in the present study

The technique described in this paper for measuring pixel flow velocities relies upon the magnetic flux density being uniform in the y direction in the flow cross section at the plane of the electrodes. To check the uniformity of the magnetic field produced by the Helmholtz coil a 48V dc power supply was connected to the two coils which were configured in parallel so that an equal current of 1.372A flowed in the same direction in each coil. A 'Hirst GM08 Gauss-meter' was then used to measure the magnetic flux density in the y direction at 179 points in the flow cross section at the plane of the electrodes. The results, which are presented graphically in Figure 2, were analysed to show that the mean measured magnetic flux density in the flow cross section was 107.33gauss, whilst the maximum and minimum measured values of the magnetic flux density were 107.89gauss and 106.52gauss, indicating the very near uniformity of the magnetic field strength.
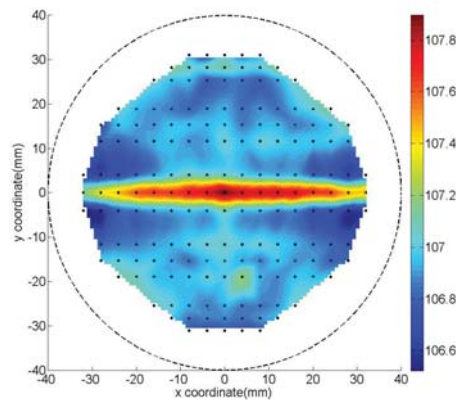

Figure 2: Distribution of magnetic flux density (gauss) in the y direction in the flow cross section at the plane of the electrodes. The dashed circular line represents the internal pipe diameter.
[NB: Measurements could not be obtained at distances greater than 31.1mm from the pipe centre due to the size of the Gaussmeter sensing head].

A 'hybrid square wave' magnetic field was generated by switching the voltage supplied to the coils, from the 48V dc power supply unit, using control signals supplied to a solid-state relay network. At any instant in time, the electrical current in both coils had the same magnitude and direction. Figure 3a is a schematic of the variation of the mean magnetic flux density $\overline{B}$ in the flow cross section with time for this 'hybrid square wave', the purpose of which was to periodically reverse the direction of the flow induced potential at each electrode, thereby minimising electrochemical effects at the electrode-water interface. The typical length of each cycle of the 'hybrid square wave' magnetic field used in the

present investigation was $0.25\,\text{s}$ and the maximum $(+\overline{B}_{\max})$ and minimum $(-\overline{B}_{\max})$ values of the mean magnetic flux density in the flow cross section (in the y direction) were $+107.33\,\text{gauss}$ and -107.33 respectively. The transient time τ_c in the magnetic field, visible in figure 3a, was caused by a transient in the current in each coil (when the coil voltage was switched) due to the coil inductance.

Each cycle of the hybrid square wave magnetic field can be divided into four segments, denoted S_1 to S_4 in Figure 3a. Figure 3b shows one cycle of the jth flow induced voltage signal $U_{x,j}$ between the jth pair of electrodes in the electrode array. For a given magnetic field cycle, mean values $(\overline{U}_{x,j})_{S1}$, $(\overline{U}_{x,j})_{S2}$, $(\overline{U}_{x,j})_{S3}$, and $(\overline{U}_{x,j})_{S4}$ were obtained from measurements of $U_{x,j}$ for each of the four signal segments S_1 to S_4. Note that $(\overline{U}_{x,j})_{S1}$, $(\overline{U}_{x,j})_{S2}$, $(\overline{U}_{x,j})_{S3}$ and $(\overline{U}_{x,j})_{S4}$ were obtained from measurements of $U_{x,j}$ made after the relevant transient (of length τ_c for S_1 and S_3) was complete. For a given magnetic field cycle, the relevant flow induced potential difference U_j required for the pixel velocity calculation was obtained from the average of the difference between the jth measured voltages when $\overline{B} = +\overline{B}_{\max}$ and $\overline{B} = 0$ and the difference between the jth measured voltages when $\overline{B} = 0$ and $\overline{B} = -\overline{B}_{\max}$ as shown in equation 9 below. Division by 996 (amplification gain) is required in equation 9 to compensate for the amplification of the differential instrumentation amplifier described above.

$$U_j = \frac{\left|(\overline{U}_{x,j})_{s1} - (\overline{U}_{x,j})_{s2}\right| + \left|(\overline{U}_{x,j})_{s3} - (\overline{U}_{x,j})_{s4}\right|}{2} \times \left\{\frac{1}{996}\right\} \tag{9}$$
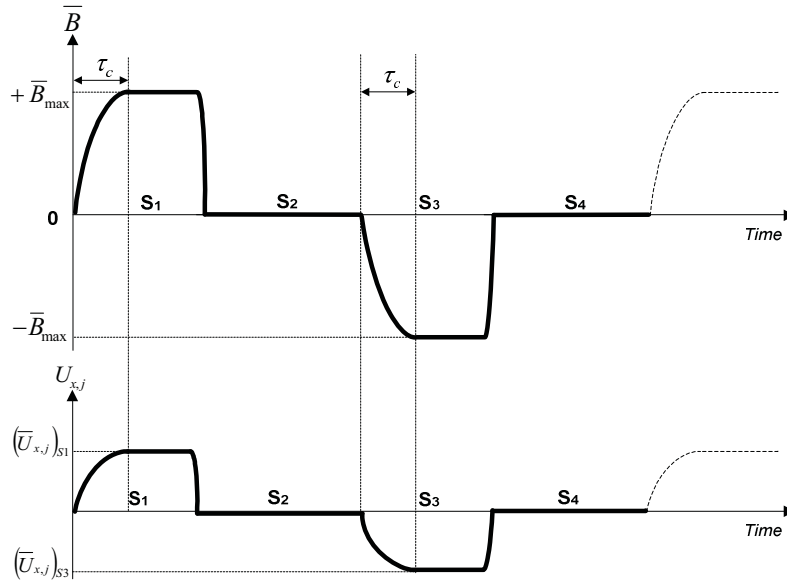

Figure 3: 3a (top) Hybrid square wave magnetic field cycle. 3b (bottom) resultant flow induced potential difference for j^{th} electrode pair.

3 EXPERIMENTAL RESULTS IN MULTIPHASE FLOW

Measurements of the local water velocity profile in a solids-in-water flow were made using the EMFM device described in section 2. The experiments were performed in the 3m long 80mm internal

diameter working section of a multiphase flow loop at the University of Huddersfield (see [10] for a more complete description of the flow loop). For the experiments described in this paper the working section was either vertical ($\theta = 0^{\circ}$) or inclined at an angle of 30° ($\theta = 30^{\circ}$) away from vertical. Electrically non-conducting spherical, plastic beads with an average diameter of 4 mm and a density of $1340.8\,\mathrm{kgm}^{-3}$ were homogenously mixed with water in a holding tank before being pumped to the base of the working section. The flow rate of the multiphase mixture was controlled by varying the speed of a multiphase pump located between the holding tank and the working section. The EMFM device described in section 2 was installed 2m away from the inlet of the working section. At each flow condition, voltages $U_{x,j}$ ($j = 1$ to 7) (see figure 4) were measured for the relevant electrode pairs over a period of 60s (with reference to section 2, this meant that values of $(\overline{U}_{x,j})_{S1}$, $(\overline{U}_{x,j})_{S2}, (\overline{U}_{x,j})_{S3}$ and $(\overline{U}_{x,j})_{S4}$ were obtained from averaging data from 240 magnetic field cycles, since each magnetic field cycle has a period of $0.25\mathrm{s}$). Results for several multiphase flow conditions are presented in figures 4 and 5. In these figures, for $\theta = 0^{\circ}$, the solids volumetric flow rate Q_s was in the range $0.51\mathrm{m}^3\mathrm{hr}^{-1}$ to $0.98\mathrm{m}^3\mathrm{hr}^{-1}$ and the water volumetric flow rate Q_w was in the range $7.89\mathrm{m}^3\mathrm{hr}^{-1}$ to $15.74\mathrm{m}^3\mathrm{hr}^{-1}$. For $\theta = 30^{\circ}$, Q_s was in the range $0.36\mathrm{m}^3\mathrm{hr}^{-1}$ to $0.75\mathrm{m}^3\mathrm{hr}^{-1}$ and Q_w was in the range $8.34\mathrm{m}^3\mathrm{hr}^{-1}$ to $13.77\mathrm{m}^3\mathrm{hr}^{-1}$. These values of Q_s and Q_w are typical of those encountered in industrial slurry monitoring application in 80mm diameter pipes.

For each flow condition investigated, the induced voltages U_j (j = 1 to 7) were calculated from the measured values of $(\overline{U}_{x,j})_{S1}$, $(\overline{U}_{x,j})_{S2}$, $(\overline{U}_{x,j})_{S3}$ and $(\overline{U}_{x,j})_{S4}$ according to equation 9 and the corresponding pixel velocities v_i (i = 1 to 7) were then calculated from these values of U_j by matrix inversion to give v_i according to equation 8. Figure 4 shows a plot of the values of U_j for each electrode pair for all of the flow conditions investigated. Figure 5 shows a plot of the reconstructed pixel velocities for all of the flow conditions investigated.
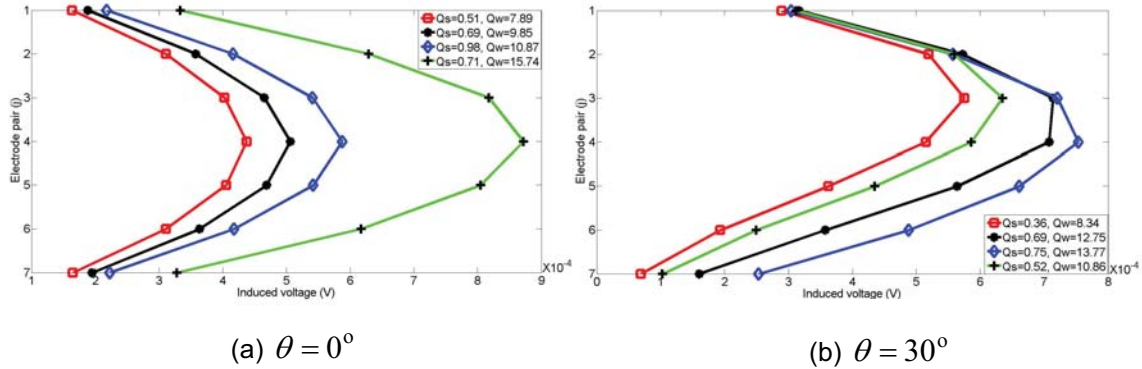

(a) $\theta = 0^{\circ}$ (b) $\theta = 30^{\circ}$

Figure 4: The induced voltages U_j for vertical and inclined solids-in-water flow

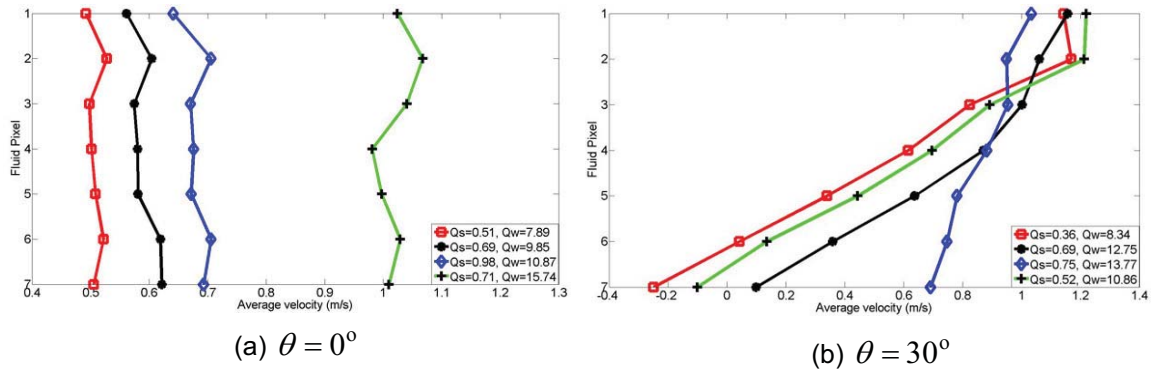(a) $\theta = 0^{\circ}$ (b) $\theta = 30^{\circ}$

Figure 5: The reconstructed pixel velocities v_i for vertical and inclined solids-in-water flow

The reconstructed velocity profiles illustrated in Figure 5(b) clearly indicate evidence of negative axial water velocity at the lower side of the inclined pipe, showing that in the seventh pixel, the water was flowing back down the pipe. Towards the upper side of the inclined pipe, the mean axial water velocity was large and positive indicating that the water was flowing quickly upward. These results agree well with visual observation of the flow undertaken using high speed filming. Previous research (e.g. [10]) has reported similar phenomena in inclined solids-in-water flows from results obtained using an intrusive six electrode local conductance velocity measurement probe. Figure 5(a) shows that for vertical solids-in-water flows the water velocity is much more uniform in the flow cross section.

4 CONCLUSIONS

This paper describes a measurement technique for mapping velocity profiles in single phase and multiphase flows. The results described in this paper are mainly relevant to flows in which the axial flow velocity varies *principally* in a single direction such as (i) flows behind partially open valves or (ii) horizontal and inclined multiphase flows in which the continuous phase is electrically conducting. However by using alternative pixel arrangements the technique can be readily adapted to flows in which the axial velocity profile variation is not principally in a single direction. A weight value theory for an electromagnetic flow meter with multiple electrodes has been implemented and proved to be a valid method for relating the mean flow velocity in a pixel to the potential differences measured between various pairs of electrodes. Moreover, this paper has used a matrix inversion method that can be combined with the weight values to reconstruct the mean velocity in each of a number of pixels from a given set of boundary potential difference measurements. In simulations, reconstructed velocities give good agreement with the reference pixel velocities and the reconstructed velocity profiles enable reasonably accurate volumetric flow estimates to be made. Experimental results for the measured water velocity profile, obtained in upward solids-in-water flows inclined at 0° and 30° to the vertical using a real multi-electrode electromagnetic flow meter, agreed well with the observed water velocity profile obtained from high speed filming. It is believed that the application of the techniques described in this paper to the measurement of highly non-uniform velocity profiles in multiphase flows is novel.

5 REFERENCES

[1]   J. Z. Wang, G. Y. Tian, and G. P. Lucas, "Relationship between velocity profile and distribution of induced potential for an electromagnetic flow meter," *Flow Measurement and Instrumentation*, vol. 18, no. 2, pp. 99-105, Apr. 2007.

[2]   H. Boris, "A novel profile-insensitive multi-electrode induction flowmeter suitable for industrial use," *Measurement*, vol. 24, no. 3, pp. 131-137, Oct. 1998.

[3]   L. J. Xu, X. M. Li, F. Dong, Y. Wang, and L. A. Xu, "Optimum estimation of the mean flow velocity for the multi-electrode inductance flowmeter," *Measurement Science and Technology*, vol. 12, pp. 1139-1146, Aug. 2001.

[4]   Mi Wang, Yixin Ma, N. Holliday, Yunfeng Dai, R. A. Williams, and G. Lucas, "A high-performance EIT system," *IEEE Sensors Journal*, vol. 5, no. 2, pp. 289- 299, Apr. 2005.

[5]   Lijun Xu, Ya Wang, and Feng Dong, "On-line monitoring of nonaxisymmetric flow profile with a multielectrode inductance flowmeter," *Instrumentation and Measurement, IEEE Transactions on*, vol. 53, no. 4, pp. 1321-1326, 2004.

[6]   E. J. Williams, "The induction of electromotive forces in a moving liquid by a magnetic field, and its application to an investigation of the flow of liquids," *Proceedings of the Physical Society*, vol. 42, pp. 466-478, Aug. 1930.

[7]   J. A. Shercliff, *the Theory of Electromagnetic Flow-Measurement*, New Ed. Cambridge University Press, 1987.

[8]   G. P. Lucas, J. Cory, R. C. Waterfall, W. W. Loh, and F. J. Dickin, "Measurement of the solids volume fraction and velocity distributions in solids–liquid flows using dual-plane electrical resistance tomography," *Flow Measurement and Instrumentation*, vol. 10, no. 4, pp. 249-258, Dec. 1999.